This is the peer reviewed version of the following article: Burzyński S., Chróścielewski J., Witkowski W., Geometrically nonlinear FEM analysis of 6-parameter resultant shell theory based on 2-D Cosserat constitutive model, ZAMM-Zeitschrift fur Angewandte Mathematik und Mechanik, Vol. 96, iss. 2 (2015), pp. 191-204, which has been published in final form at https://doi.org/10.1002/zamm.201400092. This article may be used for non-commercial purposes in accordance with Wiley Terms and Conditions for Use of Self-Archived Versions. This article may not be enhanced, enriched or otherwise transformed into a derivative work, without express permission from Wiley or by statutory rights under applicable legislation. Copyright notices must not be removed, obscured or modified. The article must be linked to Wiley's version of record on Wiley Online Library and any embedding, framing or otherwise making available the article or pages thereof by third parties from platforms, services and websites other than Wiley Online Library must be prohibited.

Geometrically nonlinear FEM analysis of 6-parameter resultant shell theory based on 2-D Cosserat constitutive model

Burzyński S., Chróścielewski J., Witkowski W.

corresponding author: wojwit@pg.gda.pl

Gdansk University of Technology,

Faculty of Civil and Environmental Engineering, Department of Structural Mechanics, 80-233 Gdańsk, Narutowicza 11/12, Poland

Key words: Cosserat constitutive equations, micropolar constants, nonlinear six-parameter shell theory, drilling rotation,

Abstract

We develop the elastic constitutive law for the resultant statically and kinematically exact, nonlinear, 6-parameter shell theory. The Cosserat plane stress equations are integrated through-the-thickness under assumption of the Reissner-Mindlin kinematics. The resulting constitutive equations for stress resultant and couple resultants are expressed in terms of two micropolar constants: the micropolar modulus G_c and the micropolar characteristic length l. Based on FEM simulations we evaluate their influence on the behaviour of shell models in the geometrically nonlinear range of deformations.

1. Introduction

Following previous papers [1][2][3]we continue study on constitutive relation for elastic shells with drilling degree of freedom. As the framework we use the nonlinear statically and kinematically exact six-parameter shell theory. The term "statically exact" means that the 2D equilibrium equations of the shell-like body are obtained in the course of direct and exact through-the-thickness integration of 3D balance laws of linear and angular momentum of the Cauchy continuum. That the shell theory is kinematically exact reflects the fact that shell kinematics follows directly from integral identity which results from the exact equilibrium equations. The resulting kinematic model is formally equivalent to the Cosserat surface with three rigidly rotating directors.

Theoretical basis can be traced back to works of Reissner [4] and Libai and Simmonds [5]. Further theoretical developments and aspects of numerical formulation can be found for instance in [6][7][8][9][10][11]

In the previous works e.g. [12][13][14][15][16][17] the constitutive relation had in some sense postulated character. In the part associated with the drilling rotation the drilling stiffness has been expressed by postulated material coefficient α_t, cf. [14].

Another approach to formulation of the material law has been proposed in [18]. Departing from the asymmetric Cauchy-type plane stress relation in the shell base, using the first order shear deformation theory (FOSD, e.g. [19] or Reissner-Mindlin kinematics) and through-the-thickness integration resulted in the equivalent single layer constitutive relation for composite shells.

Recently [20][21], we have proposed the elastoplastic J_2-type material law that has been obtained by the Reissner-Mindlin type trough-the-thickness integration of the plane stress Cosserat relation. The details of formulation and representative numerical results are presented in [20][21].

In this paper we concentrate on the elastic part of the constitutive relation proposed in [20][21]. In particular, we examine the influence of micropolar material constants on the overall behavior of shells in FEM geometrically nonlinear analysis. The approach presented here takes as its starting point the constitutive relation for plane stress Cosserat continuum, cf. for instance [22]. The constitutive relation is based on the following assumptions:

- strains are small everywhere in the shell space,
- strain measures on the reference surface are kinematically unique, which is a natural coherence with the resultant shell theory,
- strains in the shell space are derived from the natural strains measures under the assumption of the Reissner-Mindlin kinematics,
- stress resultants and couple resultants are found from strains in the shell space assuming the plane stress elastic Cosserat constitutive relation,
- the shell is sufficiently thin to assume that for every coordinate in the thickness direction the determinant μ of the shifter tensor $\mu_{\alpha\beta}$ satisfies the condition $\mu \approx 1$.

2. Kinematics of the shell

We use standard convention of indices, i.e. the Latin indices run from 1 to 3 while the Greek ones run from 1 to 2. Vectors are represented by boldface lower-case characters while tensors by boldface capital letters. Comma $(.),_{\beta} = \frac{\partial(.)}{\partial s^{\beta}}$ indicates partial differentiation with respect to the surface coordinates.

MOST WIEDZY Downloaded from mostwiedzy.pl

Assume that the undeformed shell reference surface M satisfies all necessary regularity conditions required for definition of the metric and the curvature tensors. Imagine a regular point $\boldsymbol{x} \subset M$ (see

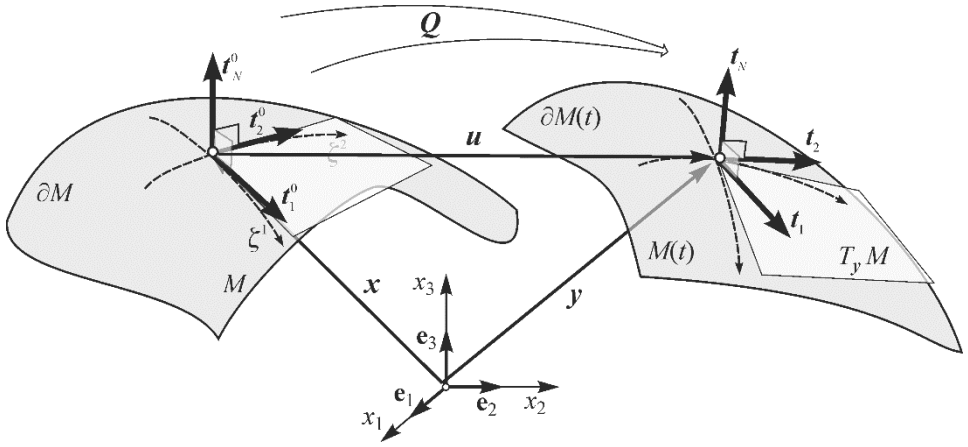

Fig. 1) at which there exists tangent space $T_{\boldsymbol{x}}M$ spanned by two vectors $\boldsymbol{t}_\beta^0 = \boldsymbol{x}_{,\beta}$, $\beta = 1,2$ with s^β as the orthogonal curvilinear arc length coordinates. The vector orthogonal to $T_{\boldsymbol{x}}M$ results from

$$\boldsymbol{t}^0 \equiv \boldsymbol{t}_3^0 = \frac{\boldsymbol{t}_1^0 \times \boldsymbol{t}_2^0}{\| \boldsymbol{t}_1^0 \times \boldsymbol{t}_2^0 \|}. \tag{1}$$

The orthogonal triad $\boldsymbol{t}_i^0(\boldsymbol{x})$ defines the microstructure tensor $\boldsymbol{T}_0 \in SO(3)$. In the present approach we assume that the triad $\boldsymbol{t}_i^0(\boldsymbol{x})$ is rigid and generates the Euclidean space endowed with the scalar product $(\boldsymbol{a}\,|\,\boldsymbol{b}) = a_i b_i$ and the norm $\|\boldsymbol{a}\| = \left(\sum_{i=1}^3 a_i^2\right)^{1/2}$.

In motion $\mathbf{u}(\boldsymbol{x}) = (\boldsymbol{u}(\boldsymbol{x}), \boldsymbol{Q}(\boldsymbol{x}))$ the current position of $\boldsymbol{x} \subset M$ and the current orientation of $\boldsymbol{t}_i^0(\boldsymbol{x})$ are given by (see

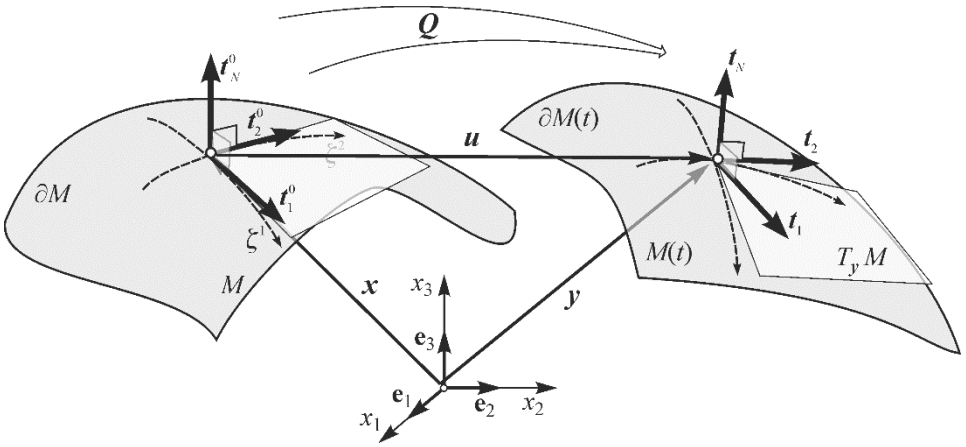

Fig. 1)

$$\boldsymbol{y}(\boldsymbol{x}) = \boldsymbol{x} + \boldsymbol{u}(\boldsymbol{x}), \quad \boldsymbol{t}_i(\boldsymbol{x}) = \boldsymbol{Q}(\boldsymbol{x})\boldsymbol{t}_i^0(\boldsymbol{x}) = \boldsymbol{Q}(\boldsymbol{x})\boldsymbol{T}_0(\boldsymbol{x})\mathbf{e}_i = \boldsymbol{T}(\boldsymbol{x})\mathbf{e}_i, \quad \boldsymbol{Q}(\boldsymbol{x}), \boldsymbol{T}_0(\boldsymbol{x}), \boldsymbol{T}(\boldsymbol{x}) \in SO(3). \tag{2}$$

MOST WIEDZY Downloaded from mostwiedzy.pl

Here $\boldsymbol{Q}(\boldsymbol{x}) \in SO(3)$ is an independent proper orthogonal tensor computed through some conveniently selected parametrization, cf. for instance [23][24] for extensive discussion. Here we use the canonical parametrization.

The definition of strain measures in the defined basis is given by

$$\boldsymbol{\varepsilon}_\beta = \boldsymbol{y}_{,\beta} - \boldsymbol{t}_\beta = \boldsymbol{u}_{,\beta} + (\mathbf{1} - \boldsymbol{Q})\boldsymbol{t}_\beta^0, \quad \delta\boldsymbol{\varepsilon}_\beta = \boldsymbol{v}_{,\beta} + \boldsymbol{y}_{,\beta} \times \boldsymbol{w}, \tag{3}$$

and in component form

$$\boldsymbol{\varepsilon}_\beta = \varepsilon_{\beta 1}\boldsymbol{t}_1 + \varepsilon_{\beta 2}\boldsymbol{t}_2 + \varepsilon_\beta \boldsymbol{t}_3. \tag{4}$$

Curvatures are obtained from the relations

$$\boldsymbol{\kappa}_\beta = \mathrm{axl}(\boldsymbol{Q}_{,\beta}\boldsymbol{Q}^{\mathrm{T}}), \quad \delta\boldsymbol{\kappa}_\beta = \boldsymbol{w}_{,\beta}, \tag{5}$$

where the axial vector of the skew tensor is defined with operator axl. The components of $(5)_1$ are given by

$$\boldsymbol{\kappa}_\beta = \boldsymbol{t}_3 \times (\kappa_{\beta 1}\boldsymbol{t}_1 + \kappa_{\beta 2}\boldsymbol{t}_2) + \kappa_\beta \boldsymbol{t}_3. \tag{6}$$

For the convenience we gather the components (4) and (6) in vector

$$\boldsymbol{\varepsilon} = \{\varepsilon_{11}\ \varepsilon_{22}\ \varepsilon_{12}\ \varepsilon_{21} | \varepsilon_1\ \varepsilon_2 \| \kappa_{11}\ \kappa_{22}\ \kappa_{12}\ \kappa_{21} | \kappa_1\ \kappa_2\}^T = \{\boldsymbol{\varepsilon}_m | \boldsymbol{\varepsilon}_s \| \boldsymbol{\varepsilon}_b | \boldsymbol{\varepsilon}_d\}^T, \tag{7}$$

where labels *m, s, b, d* denote respectively: the membrane, shear, bending and drilling part. Correspondingly we formulate the vector

$$\boldsymbol{s} = \{N^{11}N^{22}N^{12}N^{21} | Q^1Q^2 \| M^{11}M^{22}M^{12}M^{21} | M^1M^2\}^T = \{\boldsymbol{s}_m | \boldsymbol{s}_s \| \boldsymbol{s}_b | \boldsymbol{s}_d\}^T, \tag{8}$$

of components of the stress resultants

$$\boldsymbol{n}^\beta = N^{\beta 1}\boldsymbol{t}_1 + N^{\beta 2}\boldsymbol{t}_2 + Q^\beta \boldsymbol{t}_3, \tag{9}$$

and stress couples

$$\boldsymbol{m}^\beta = \boldsymbol{t}_3 \times (M^{\beta 1}\boldsymbol{t}_1 + M^{\beta 2}\boldsymbol{t}_2) + M^\beta \boldsymbol{t}_3. \tag{10}$$

The concise statement of the weak form of the boundary value problem reads [25][26]: given the external resultant force and couple vector fields $\boldsymbol{f}(\boldsymbol{x},t)$ and $\boldsymbol{c}(\boldsymbol{x},t)$ on $\boldsymbol{x} \in M$, $\boldsymbol{n}^*(\boldsymbol{x},t)$ and $\boldsymbol{m}^*(\boldsymbol{x},t)$ along ∂M_f, $\boldsymbol{f}_\Gamma(\boldsymbol{x}_\Gamma,t)$ find $\mathbf{u}(\boldsymbol{x}) = (\boldsymbol{u}(\boldsymbol{x}), \boldsymbol{Q}(\boldsymbol{x}))$ on the configuration space $C(M, E^3 \times SO(3))$ such that for any continuous kinematically admissible virtual vector field $\mathbf{w} \equiv (\boldsymbol{v}, \boldsymbol{w})$ the following principle of virtual work is satisfied:

$$G[\mathbf{u};\mathbf{w}] = \iint_M [\boldsymbol{n}^\beta \cdot (\boldsymbol{v}_{,\beta} + \boldsymbol{y}_{,\beta} \times \boldsymbol{w}) + \boldsymbol{m}^\beta \cdot \boldsymbol{w}_{,\beta}]\, da - \iint_M (\boldsymbol{f} \cdot \boldsymbol{v} + \boldsymbol{c} \cdot \boldsymbol{w})\, da - \int_{\partial M_f} (\boldsymbol{n}^* \cdot \boldsymbol{v} + \boldsymbol{m}^* \cdot \boldsymbol{w})\, ds = 0 \tag{10}$$

MOST WIEDZY Downloaded from mostwiedzy.pl

Here it is implicitly assumed that the kinematic boundary conditions $\boldsymbol{u}(\boldsymbol{x}) = \boldsymbol{u}^*(\boldsymbol{x})$ and $\boldsymbol{Q}(\boldsymbol{x}) = \boldsymbol{Q}^*(\boldsymbol{x})$ are satisfied along the complementary part $\partial M_d = \partial M \setminus \partial M_f$ of the shell boundary. Furthermore the virtual vector fields are kinematically admissible if $\boldsymbol{v}(\boldsymbol{x}) = \boldsymbol{0}$ and $\boldsymbol{w}(\boldsymbol{x}) = \boldsymbol{0}$ along ∂M_d.

3. Constitutive relation

In this section we derive the 2D constitutive relation of which the general form is

$$\mathbf{s} = \mathbf{C}\boldsymbol{\varepsilon}. \tag{11}$$

To some extent the derivations presented in the previous paragraphs, has the features of the so-called derived approach understood here as direct descent from 3D Cauchy continuum to 2D Cosserat surface. The formulation, as discussed so far, is free of any kinematical assumptions. Initially, cf. for instance [12][13], the constitutive relations within the present shell theory had, in some sense, postulated character – see the third column of table 1. This concerns, among other things, the drilling component (6DOF) which is defined as dependent on material coefficient α_t – see two last rows of table 1.

Due to the lack of theoretical base for assessment of α_t values from 3D experiments, the role of material coefficient α_t has been studied numerically e.g. [12], [13] both from physical point of view understood as its contribution to drilling couples M^1 and M^2, and from numerical standpoint that is its influence on numerical stability. As a result a bound $\alpha_t <\sim 1$ has been established.

It is worthy of note that upon reduction of the physical problem of shell (1)-(6) to plane stress problem the non-vanishing components (7) and (8) are

$$\{\boldsymbol{\varepsilon}_m | \boldsymbol{\varepsilon}_d\}^T = \{\varepsilon_{11}\ \varepsilon_{22}\ \varepsilon_{12}\ \varepsilon_{21} | \kappa_1\ \kappa_2\}^T,\ \{\mathbf{s}_m | \mathbf{s}_d\}^T = \{N^{11}\ N^{22}\ N^{12}\ N^{21} | M^1 M^2\}^T \tag{12}$$

Equations (12) are valid for plane stress Cosserat continuum, cf. for example [27] This fact constitutes the foundation of our approach.

As indicated in the introduction, the components of $\mathbf{C}$ are derived from through the thickness integration of micropolar plane stress assumed in shell layer. We represent $\mathbf{C}$ in a general manner as, cf. [20][21].

$$\mathbf{C} = \left[\begin{array}{c|c|c|c} \mathbf{A}_{mm} & \mathbf{0} & \mathbf{B}_{mb} & \mathbf{0} \\ \hline \mathbf{0} & \mathbf{D}_{ss} & \mathbf{0} & \mathbf{0} \\ \hline \mathbf{B}_{mb}^T & \mathbf{0} & \mathbf{E}_{bb} & \mathbf{0} \\ \hline \mathbf{0} & \mathbf{0} & \mathbf{0} & \mathbf{H}_{dd} \end{array}\right]. \tag{13}$$

The respective components of asymmetric strain and stress tensor in shell layer are collected in vectors

MOST WIEDZY Downloaded from mostwiedzy.pl

$$\boldsymbol{\varepsilon}=\begin{Bmatrix}\boldsymbol{\varepsilon}_m\\ \hdashline \boldsymbol{\varepsilon}_d\end{Bmatrix}=\begin{Bmatrix}\varepsilon_{11}\\ \varepsilon_{22}\\ \varepsilon_{12}\\ \hdashline \varepsilon_{21}\\ \varepsilon_1\\ \varepsilon_2\end{Bmatrix}=\begin{Bmatrix}\varepsilon_{11}\\ \varepsilon_{22}\\ \varepsilon_{12}\\ \hdashline \varepsilon_{21}\\ \kappa_1\cdot l\\ \kappa_2\cdot l\end{Bmatrix},\qquad \boldsymbol{\sigma}=\begin{Bmatrix}\boldsymbol{\sigma}_m\\ \hdashline \boldsymbol{\sigma}_d\end{Bmatrix}=\begin{Bmatrix}\sigma_{11}\\ \sigma_{22}\\ \sigma_{12}\\ \hdashline \sigma_{21}\\ \sigma_1\\ \sigma_2\end{Bmatrix}=\begin{Bmatrix}\sigma_{11}\\ \sigma_{22}\\ \sigma_{12}\\ \hdashline \sigma_{21}\\ m_1/l\\ m_2/l\end{Bmatrix}. \tag{14}$$

Components collected in (14) have same meaning as those in (12). In (14) l is the micropolar characteristic length (material parameter). The elastic constitutive relation of the Cosserat plane stress is assumed as

$$\boldsymbol{\sigma}=\mathbf{C}_{cs}\boldsymbol{\varepsilon}\,. \tag{15}$$

The particular form of (15) used in this paper is derived from [27] for plane stress (cf. also [22]), i.e.

$$\mathbf{C}_{cs}=\left[\begin{array}{cccc:cc} Gc_1 & Gc_2 & 0 & 0 & 0 & 0\\ Gc_2 & Gc_1 & 0 & 0 & 0 & 0\\ 0 & 0 & G+G_c & G-G_c & 0 & 0\\ 0 & 0 & G-G_c & G+G_c & 0 & 0\\ \hdashline 0 & 0 & 0 & 0 & 2G & 0\\ 0 & 0 & 0 & 0 & 0 & 2G \end{array}\right]=\left[\begin{array}{c:c} \mathbf{C}_{mm} & \mathbf{0}\\ \hdashline \mathbf{0} & \mathbf{C}_{dd}\end{array}\right]. \tag{16}$$

Material parameters in (16) are the Kirchhoff modulus G, Poisson's ratio v and the micropolar modulus G_c. Additionally $c_1=2(1+v)\big/(1-v^2)$ and $c_2=vc_1$. The characteristic length is incorporated into vectors $(14)_{1,2}$ to render their physical dimension the same. It can be moved into elastic operator $\mathbf{C}$ to obtain

$$\mathbf{C}_{dd}=\begin{bmatrix}2Gl^2 & 0\\ 0 & 2Gl^2\end{bmatrix}. \tag{17}$$

To proceed further we employ from now on the Reissner-Mindlin kinematical assumptions. Note that the characteristic length l induces an extra stiffness into the model, not present in the classical Reissner-Mindlin model. Strains $\mathbf{e}$ in the shell space are calculated from known shell strains $\boldsymbol{\varepsilon}$ (3) and (5) as:

$$\mathbf{e}_m=\boldsymbol{\varepsilon}_m+\zeta\boldsymbol{\varepsilon}_b\,, \tag{18}$$

where ζ is coordinate through thickness of a shell h_0 which varies from $-h^-$ to h^+. Symbols h^- and h^+ denotes the position of the bottom and upper face of the 3D shell-like body, respectively.

The drilling component is assumed here

$$\mathbf{e}_d=\boldsymbol{\varepsilon}_d\cdot l\,. \tag{19}$$

MOST WIEDZY Downloaded from mostwiedzy.pl

In the remainder of this section we assume that the determinant μ of the shifter tensor $\mu_{\alpha\beta}$ satisfies the condition $\mu \approx 1$ (which is true only for thin shells). Hence we obtain for membrane, bending and drilling resultants the following equations, respectively:

$$\mathbf{s}_m = \int_{-h^-}^{+h^+} \boldsymbol{\sigma}_m d\zeta = \int_{-h^-}^{+h^+} [\mathbf{C}_{mm}(\boldsymbol{\varepsilon}_m + \zeta \boldsymbol{\varepsilon}_b)\, d\zeta = \int_{-h^-}^{+h^+} \mathbf{C}_{mm}\boldsymbol{\varepsilon}_m\, d\zeta\,, \tag{20}$$

$$\mathbf{s}_b = \int_{-h^-}^{+h^+} \boldsymbol{\sigma}_m \zeta\, d\zeta = \int_{-h^-}^{+h^+} [\mathbf{C}_{mm}(\zeta\boldsymbol{\varepsilon}_m + \zeta^2 \boldsymbol{\varepsilon}_b) d\zeta = \int_{-h^-}^{+h^+} \mathbf{C}_{mm}\zeta^2\boldsymbol{\varepsilon}_b d\zeta = \frac{h_0^3}{12}\mathbf{C}_{mm}\boldsymbol{\varepsilon}_b\,, \tag{21}$$

$$\mathbf{s}_d = \int_{-h^-}^{+h^+} l\cdot\boldsymbol{\sigma}_d\, d\zeta = \int_{-h^-}^{+h^+} l^2\cdot\mathbf{C}_{dd}\boldsymbol{\varepsilon}_d d\zeta = h_0 l^2\cdot\mathbf{C}_{dd}\boldsymbol{\varepsilon}_d\,. \tag{22}$$

Shear part is defined as

$$\mathbf{s}_s = \mathbf{D}_{ss}\boldsymbol{\varepsilon}_s = \begin{bmatrix} Gh_0\alpha_S & 0 \\ 0 & Gh_0\alpha_S \end{bmatrix}\boldsymbol{\varepsilon}_s\,, \tag{23}$$

with shear coefficient assumed here as $\alpha_S = \frac{5}{6}$. In the above formulae we introduced coefficients $C = \dfrac{Eh_0}{1-\nu^2}$, $D = \dfrac{Eh_0^3}{12(1-\nu^2)}$ as the tension stiffness and bending stiffness, respectively. Following [28] we use $N^2 = \dfrac{G_c}{G+G_c} \Rightarrow G_c = G\dfrac{N^2}{1-N^2} \Rightarrow N^2 = \dfrac{1}{2} \Rightarrow G_c = G$, known as the Cosserat coupling number.

In (19) we have assumed that drilling couples (22) depend only on $\boldsymbol{\varepsilon}_d$. Recently Pietraszkiewicz and Konopińska [7] have shown that, under some conditions, the drilling couples depend also on membrane strain components.

Summarizing, the nonzero components of elastic operator $\mathbf{C}$ in (13) are explicitly given as:

$$\mathbf{A}_{mm} = \begin{bmatrix} C & \nu C & 0 & 0 \\ \nu C & C & 0 & 0 \\ 0 & 0 & \dfrac{C(1-\nu)}{2(1-N^2)} & \dfrac{C(1-\nu)(1-2N^2)}{2(1-N^2)} \\ 0 & 0 & \dfrac{C(1-\nu)(1-2N^2)}{2(1-N^2)} & \dfrac{C(1-\nu)}{2(1-N^2)} \end{bmatrix}, \quad \mathbf{D}_{ss} = \begin{bmatrix} G\alpha_S & 0 \\ 0 & G\alpha_S \end{bmatrix}, \tag{24}$$

MOST WIEDZY Downloaded from mostwiedzy.pl

$$\mathbf{E}_{bb}=\begin{bmatrix} D & \nu D & 0 & 0 \\ \nu D & D & 0 & 0 \\ 0 & 0 & \dfrac{D(1-\nu)}{2\left(1-N^2\right)} & \dfrac{D(1-\nu)\left(1-2N^2\right)}{2\left(1-N^2\right)} \\ 0 & 0 & \dfrac{D(1-\nu)\left(1-2N^2\right)}{2\left(1-N^2\right)} & \dfrac{D(1-\nu)}{2\left(1-N^2\right)} \end{bmatrix}, \quad \mathbf{H}_{dd}=\begin{bmatrix} 2Gh_0l^2 & 0 \\ 0 & 2Gh_0l^2 \end{bmatrix}. \tag{25}$$

Table 1 presents the comparison between resultants components derived in the present approach and used so-far in e.g. [12][13][14][15]. In particular it can be shown that for $N=\dfrac{\sqrt{2}}{2}$ we have the following identities

$$\alpha_t D(1-\nu)=2Gh_0l^2 \quad \Leftrightarrow \quad \alpha_t \frac{Eh_0^3}{12(1-\nu^2)}(1-\nu)=2\frac{E}{2(1+\nu)}h_0l^2 \tag{26}$$

which provide the relation

$$l=\sqrt{\frac{\alpha_t}{12}}h_0 \quad \Leftrightarrow \quad \alpha_t=12\left(\frac{l}{h_0}\right)^2 \tag{27}$$

Relation (27) throws new light on the meaning of α_t. Namely, it shows explicitly that α_t has clear interpretation of material parameter connected with micropolar length $l=\sqrt{\dfrac{\alpha_t}{12}}h_0$. Hence, under given $N=\dfrac{\sqrt{2}}{2}$ the influence of l on the results will have the same character as that of α_t (cf. for instance [12][13]) scaled by a factor $\alpha_t=12\left(\dfrac{l}{h_0}\right)^2$. Therefore, based on the previous experiences, it can be argued that $l=\sqrt{\dfrac{\alpha_t}{12}}h_0$ has strongest influence (in comparison with α_t alone) for $l>1$ and weaker if $l<1$.

As far as the values of N are concerned Neff [11][29][30][31][32][33][34] have rigorously obtained well-posedness results for the geometrically nonlinear planar shell formulation which is identical to our setting in the planar case.

From purely formal viewpoint $N=N(G,G_c)$ which arguments are from ranges $G\in[0,\infty]$ and $G_c\in[0,\infty]$. In the present case of linear elastic homogenous material G is expressed by E and ν. And hence the area of research is confined to $G_c\in[0,\infty]$.

MOST WIEDZY Downloaded from mostwiedzy.pl

It has been shown theoretically and practically [35], that $N=0$ ($G_c=0$) is a valid parameter choice. However, in our implementation letting $N=0$ yields two pairs of constitutive relations, namely: N^{12} with N^{21} and M^{12} with M^{21} identical and hence are not linearly independent, see Table 1. Thus, the constitutive matrix becomes singular and the theory is no longer 6-parameter shell theory. On the other hand, $N=1$ (excluding impossible case $G=0$) corresponds to $G_c \to \infty$. This is the case of a constrained Cosserat model: continuum rotations and microrotations coincide. This implies that constitutive equations for N^{12}, N^{21}, M^{12}, M^{21} tend to infinity. Again the theory is not 6-parameter shell theory. In this way we obtain the limit case ($N=0$, $N=1$) where some of the parameters are not determined in the framework of complete i.e. 6-parameter shell theory. Therefore, in our implementation we assume that $0<N<1$.

4. Examples

It is seen from equations (24) and (25) that the shell resultants depend on two micropolar constants i.e.: $N^2=\dfrac{G_c}{G+G_c}$ and the characteristic length l. In this section we investigate, by means of FEM, their influence on the overall geometrically nonlinear response of shell structures in terms of equilibrium paths and number of iterations necessary to satisfy prescribed convergence criteria. For the selected load level we study influence of N and l on the representative displacement or critical force. Similar study may be found for example in [28] for 3-dimensional solid formulation. As FEM code we use our own Fortran code with implemented shell finite elements denoted as CAM [12][13] which are C^0 Lagrangian type elements with 6 dofs at each node. Interpolation on $SO(3)$ group is performed using special algorithm as described in [12][18]. The solver is parallelized using [38].

All the simulations presented below ale obtained with 16-node elements with full Gaussian quadrature (FI) in the element's surface. The reference solutions are computed using the material law presented in e.g. [12][13][14][15][16].

MOST WIEDZY Downloaded from mostwiedzy.pl

4.1. Pinched hemisphere, smooth shell

As the first example we consider pinched hemisphere with a hole, see

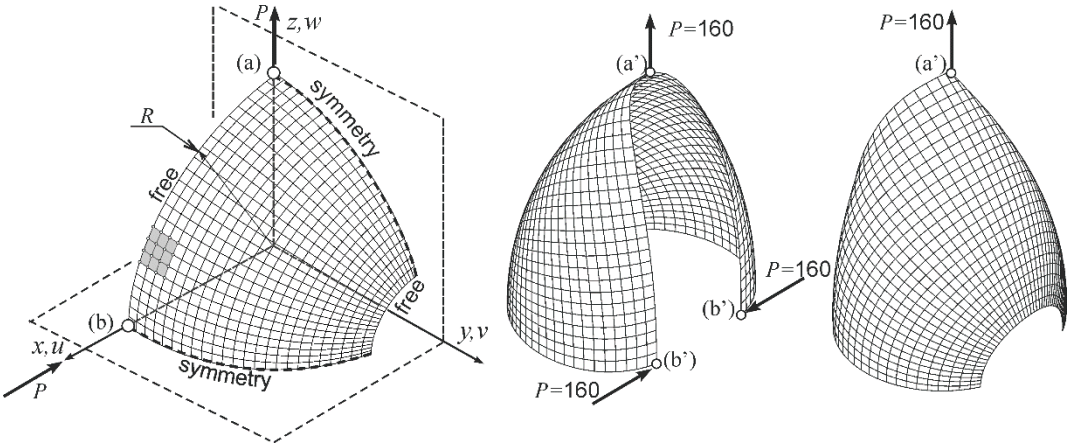

Fig. 2., cf for instance [36]. The following data is used in the analysis: $R=10$, $h_0=0.04$, $\alpha=18^{o}$, $E=6.825\times10^{7}$, $\nu=0.3$, $P_{ref}=10$, $P(\lambda)=\lambda P_{ref}$. Micropolar constants are taken as $N=\left\{0.1;\frac{\sqrt{2}}{2};0.9\right\}$ and characteristic micropolar length is taken as the ratio to the shell thickness $\frac{l}{h_0}=\left\{\frac{1}{1000};\frac{1}{100};\frac{1}{10};1;10;100\right\}$. The parameters of the reference solution are set in Table 2.

As it can be observed from

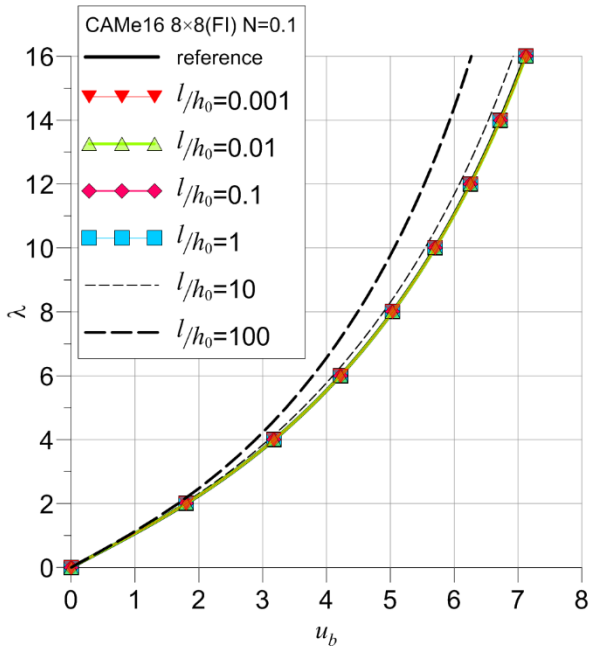

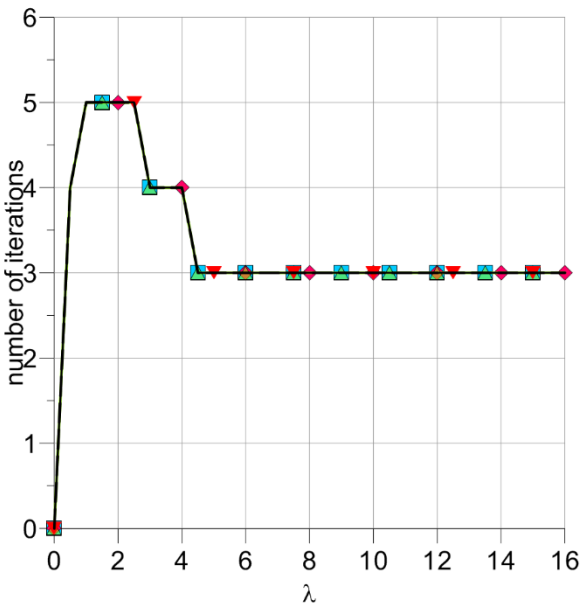

MOST WIEDZY Downloaded from mostwiedzy.pl

Fig. 3,

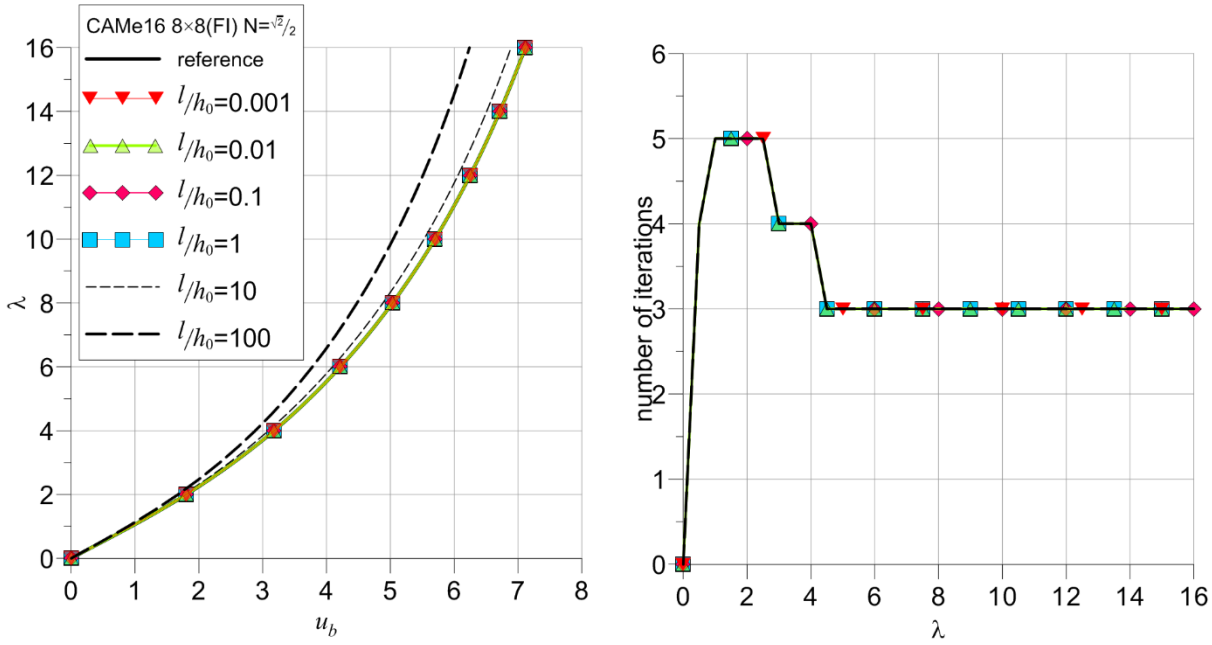

Fig. 4 and

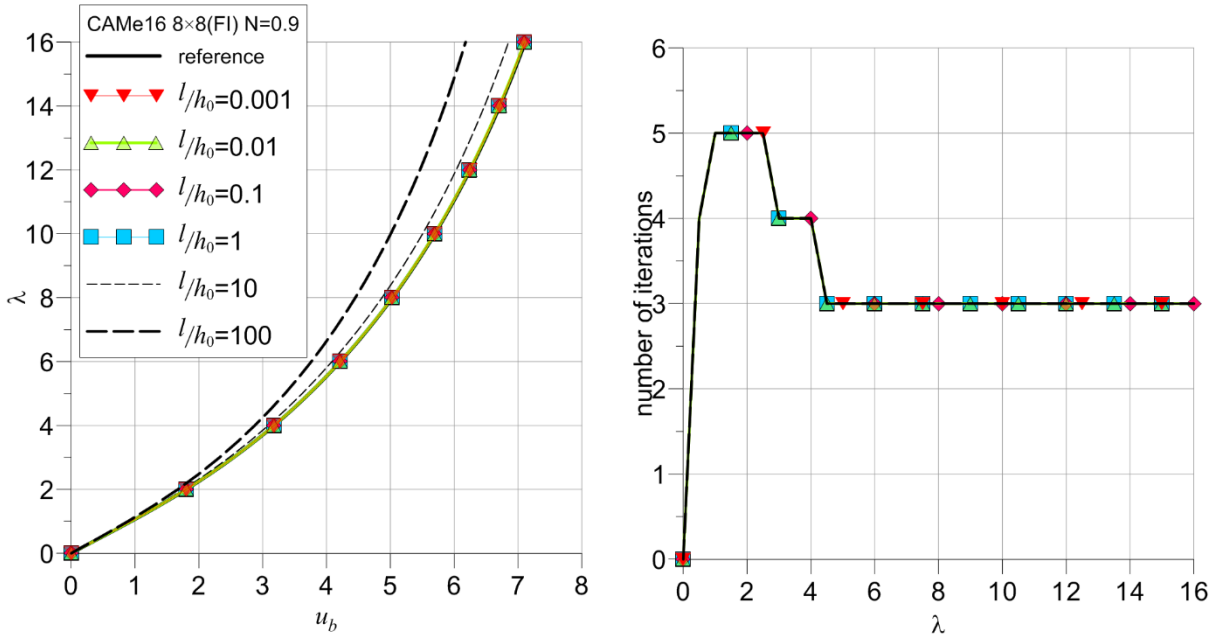

Fig. 5, the results do not differ significantly with regard to the equilibrium curves and number of iterations. The common aspect visible in all solutions is that for $\frac{l}{h_0} \leq 1$ the equilibrium curves are essentially indistinguishable. On the other hand, values of $\frac{l}{h_0} > 1$ are responsible for stiffening effect. This is clearly portrayed in

MOST WIEDZY Downloaded from mostwiedzy.pl

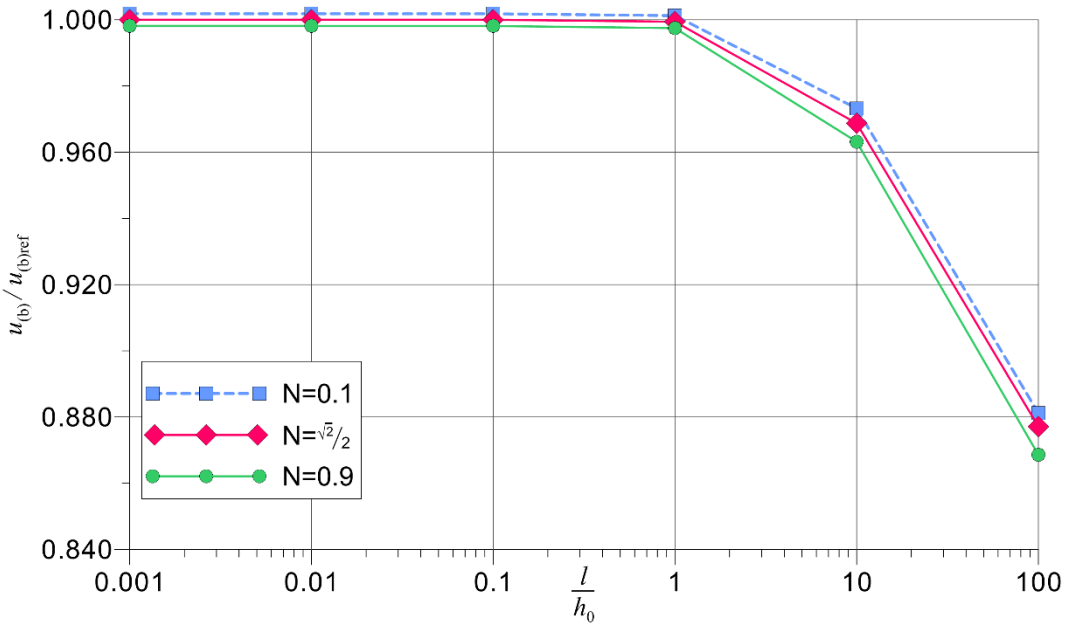

Fig. 6 where computed values of u_b are normalized with respect to $u_{(b)ref}$. Our presentation in

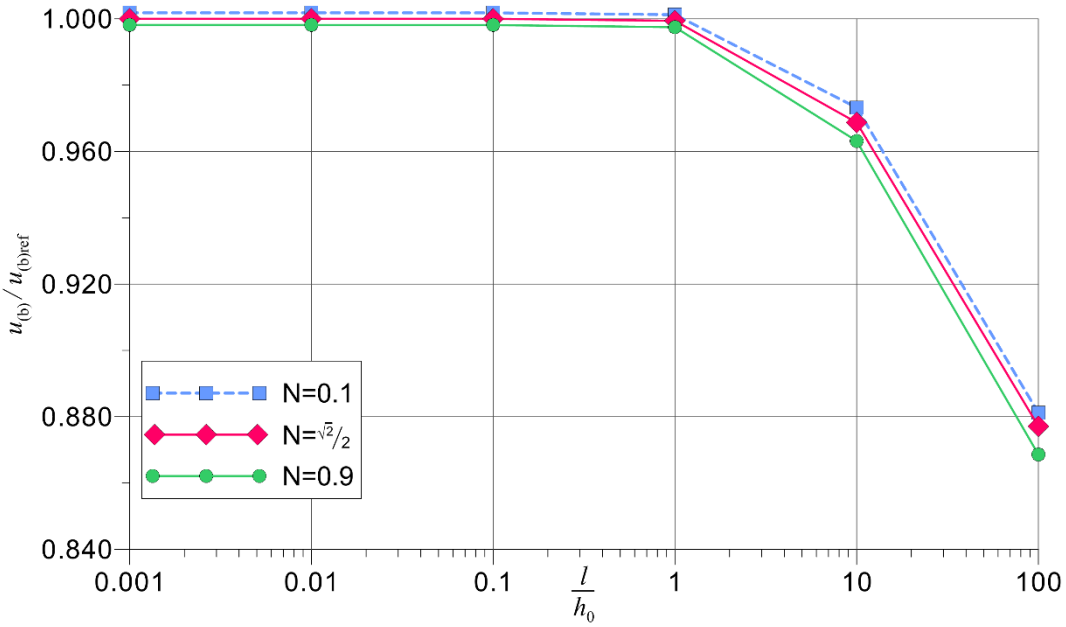

Fig. 6 follows closely that from [12][13][28]. In the latter reference the authors identified three zones of results. The first one contains the results that have character of linear Cauchy elasticity with no size effects present. In the second zone, which is a transition zone, the size effects are observable. The last zone shows results for which the microrotation is nearly constant. In this spirit, we have been able to identify in

MOST WIEDZY Downloaded from mostwiedzy.pl

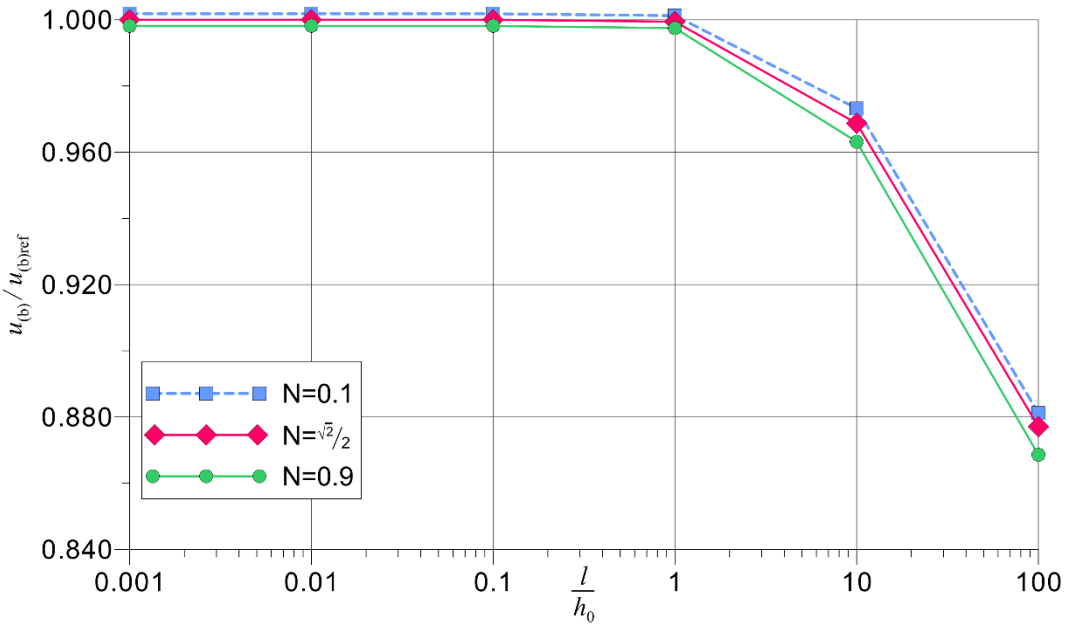

Fig. 6 the following zones: the first one for $\sim \frac{1}{100} \leq \frac{l}{h_0} \leq \sim 1$ and the transition zone $\sim 1 \leq \frac{l}{h_0} \leq \sim 100$. Due to convergence issues have not been able to obtain the results in the third zone.

4.2. Hyperbolic paraboloidal shell, smooth shell

We analyze bending deformation of free (without boundary condition) hyperbolic paraboloidal shell, see

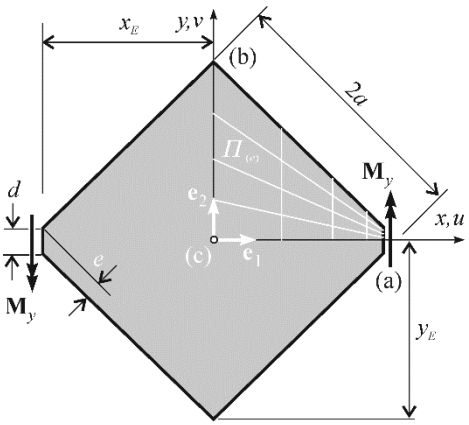

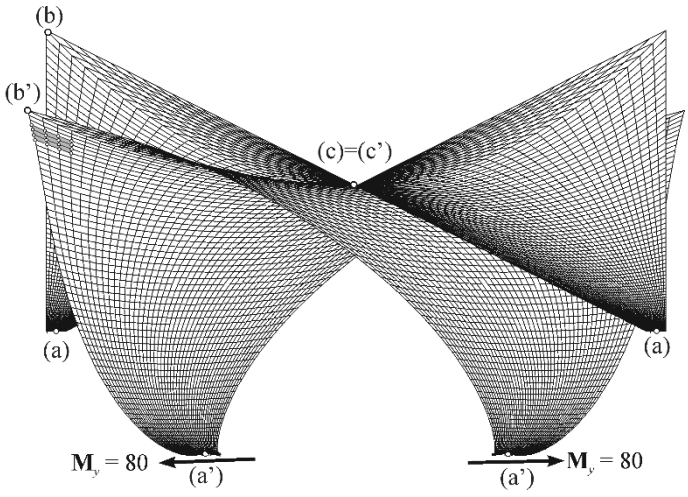

MOST WIEDZY Downloaded from mostwiedzy.pl

Fig. 7, cf. for example [18][37]. The analyzed shell is subjected to the action of two bending moments acting on the "cut" edge, see

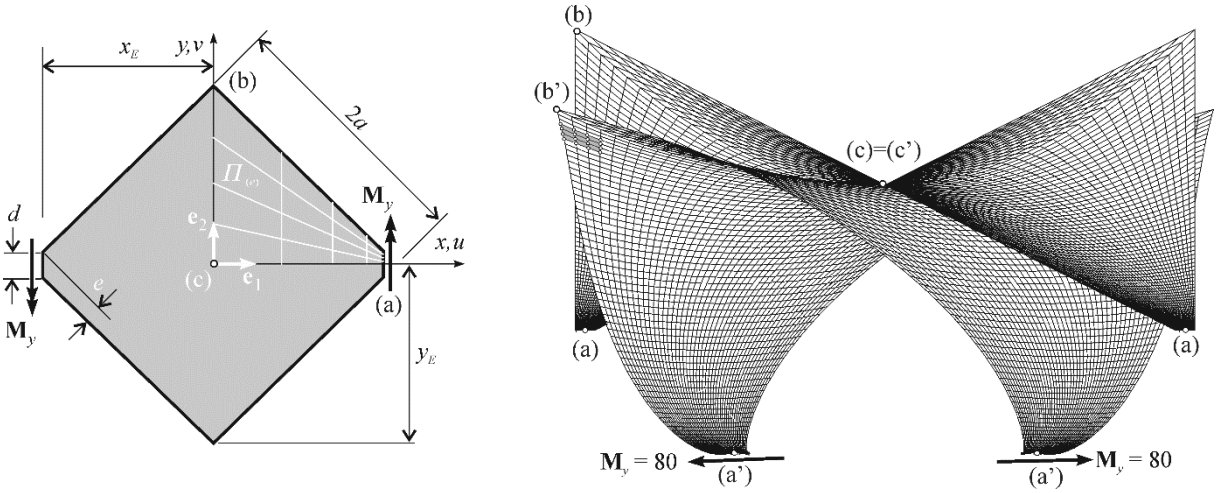

Fig. 7a. The loads are self-equilibrated. The importance of this example results from the fact that the finite elements in the initial configuration are warped. This fact can cause serious changes in the solution for some shell elements, see for instance section 14 of [39].

The following data is used: $E_1 = 10^5$, $\nu = 0.25$ $a = 10$, $c = 5$, $\sqrt{2}d = 1.25$, $h_0 = 0.18$. The proportional load $\mathbf{M}_y(\lambda) = \lambda \boldsymbol{M}_{ref}$ is self-equilibrated with respect to the reference load taken as the moment distributed along the cut edge $\boldsymbol{M}_{ref} = m_0 \int_0^d ds_0(y) \boldsymbol{e}_2$, $m_0 = 5$. In calculations, symmetry conditions are used and vertical translation of point c is also constrained. The latter constraint is formal since it is associated with reaction that must be equal to zero (due to self-equilibrated loads) that provides condition for assessing the correctness of the solution. The characteristics of the reference solution are given in Table 3.

While in the previous example the ratios $\frac{l}{h_0} = \left\{\frac{1}{1000}; \frac{1}{100}; \frac{1}{10}; 1; 10; 100\right\}$ and values of $N = \left\{0.1; \frac{\sqrt{2}}{2}; 0.9\right\}$ had no influence on the solution convergence (measured in number of iterations),

MOST WIEDZY Downloaded from mostwiedzy.pl

here the situation is entirely different. This is clearly visible in

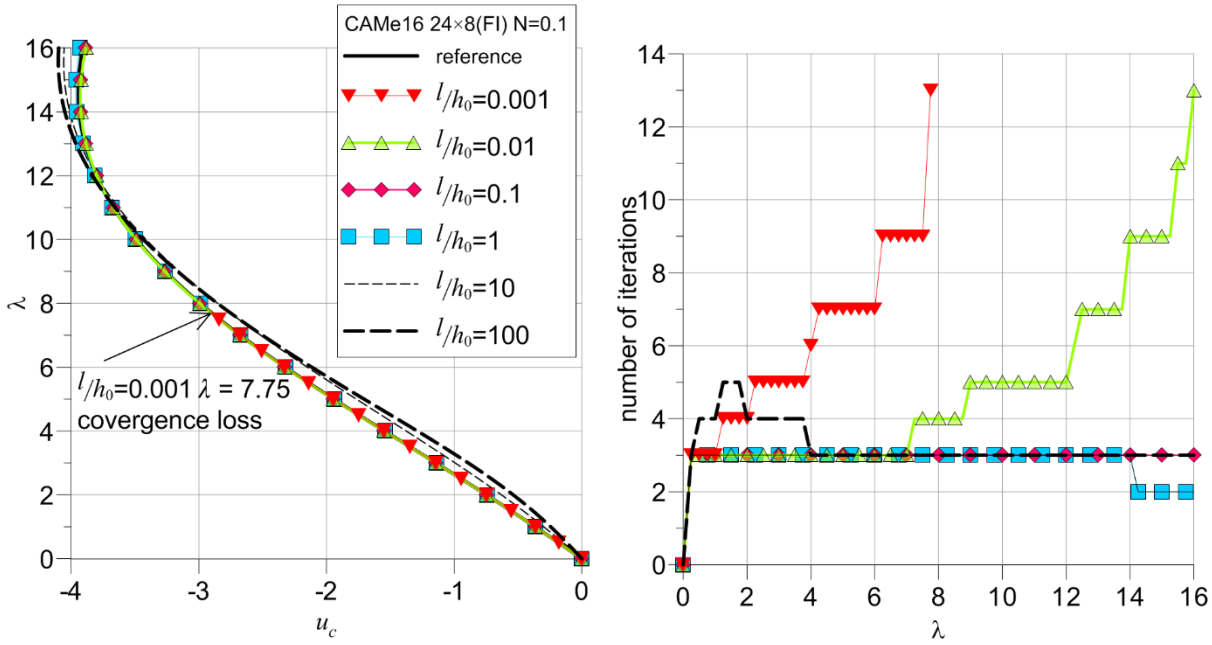

Fig. 8 for $N=0.1$ where the curve for $\frac{l}{h_0}=\frac{1}{1000}$ suddenly breaks at $\lambda=7.75$. Using $N=\left\{\frac{\sqrt{2}}{2};0.9\right\}$ improves the convergence for the whole range of $\frac{l}{h_0}$ although as it is shown in Fig. 9 the number of iterations for $\frac{l}{h_0}=\frac{1}{1000}$ grows as much as 13 towards the end of the simulation.

4.3. Torsional buckling of thin walled I-beam column, irregular shell

This example shows the natural potential of the underlying shell theory and accompanying shell elements to study irregular shell structures containing orthogonal intersections of branches. We investigate nonlinear torsional buckling of I-beam column [16], see Fig. 12. We take into account symmetry with respect to the beam length. We assume $E=2.1\times10^6$ kPa, $\nu=0.3$, $L=4$ m, $h=0.01$ m, $H=B=0.2$ m. As shown in Table 1 of [16] critical load of the torsional buckling estimated using (2+2+2)×20 CAMe16(FI) elements is $P_{cr}=3.329$ MN. In this example the reference values are given in Table 4.

The analysis revealed, see Fig. 13, Fig. 14 and Fig. 15 and Fig. 16, that for ratios $\frac{1}{1000}\le\frac{l}{h_0}\le1$, regardless of the values of $N=\left\{0.1;\frac{\sqrt{2}}{2};0.9\right\}$ critical load of the torsional buckling lays in the first zone, i.e. size effect plays negligible role. Moreover, the values of $\sim\frac{1}{1000}\le\frac{l}{h_0}\le\sim 1$ have no

MOST WIEDZY Downloaded from mostwiedzy.pl

substantial influence on the convergence of nonlinear solution. With the growth of $\frac{l}{h_0}$ the structure becomes stiffer and the corresponding value of critical load also increases. For $\sim 1 \leq \frac{l}{h_0} \leq\sim 10$ the transition zone appears, see Fig. 16. However, we were not able to find the values of critical load for $\frac{l}{h_0} >\sim 10$. Equilibrium paths, see Fig. 13, Fig. 14 and Fig. 15, do not exhibit the shape typical for structure with imperfection. Corresponding curves that denote iteration numbers needed to satisfy convergence criteria in this case are (almost) stable i.e. only one iteration is necessary.

5. Conclusions

The complete formulation of the Cosserat-type elastic material law appropriate for the resultant 6-parameter shell theory is presented. The equations have been obtained from the Cosserat plane stress relation that is integrated in the thickness direction under assumptions of Reissner-Mindlin kinematics. The obtained formulae contain explicitly two material parameters of Cosserat continuum, i.e. the micropolar modulus G_c and the characteristic micropolar length l. The numerical results for thin shells obtained in geometrically nonlinear regime support the following conclusions:

- due to numerical reasons we assume limit the values of N so that $0 < N < 1$ to avoid singularity of the constitutive matrix $\mathbf{C}$,
- the micropolar modulus G_c has smaller influence on the results in comparison with the influence of the characteristic micropolar length l;
- depending on l/h_0 ratio we have shown that the results belong to the zones indentified in [28];
- for $l/h_0 > 10$ we have observed substantial over-stiffening behavior of the analyzed shells in FEM simulations,
- if $0 < l/h_0 < 0.1$ the over-stiffening is not visible.

Acknowledgements

Parallel solver for CAM elements is developed on the basis of HSL [38] a collection of Fortran codes for large-scale scientific computation, http://www.hsl.rl.ac.uk. Stanisław Burzyński is supported by grant DEC-2012/05/D/ST8/02298, National Science Centre of Poland.

Bibliography

[1] H. Altenbach and V.A. Eremeyev, On the linear theory of micropolar plates, Z. Angew. Math. Mech. **89**, 242–256 (2009).

[2] J. Chróścielewski and W. Witkowski, FEM analysis of Cosserat plates and shells based on some constitutive relations, Z. Angew. Math. Mech. **91**, 400–412 (2011).

MOST WIEDZY Downloaded from mostwiedzy.pl

[3] J. Chróścielewski and W. Witkowski, On some constitutive equations for micropolar plates, Z. Angew. Math. Mech. **90**, 53–64 (2010).

[4] E. Reissner, Linear and nonlinear theory of shells. In: Thin Shell Structures, edited by Y.C. Fung and E.E. Sechler, 29–44 (Prentice-Hall, Englewood Cliffs 1974).

[5] A. Libai and J.G. Simmonds, The Nonlinear Theory of Elastic Shells, 2nd edn, (Cambridge University Press, Cambridge, 1998).

[6] V. Konopińska and W. Pietraszkiewicz, Exact resultant equilibrium conditions in the non-linear theory of branching and self-intersecting shells, Int. J. Solids Struct. **44**, 52–369 (2007).

[7] W. Pietraszkiewicz and V. Konopińska, Drilling couples and refined constitutive equations in the resultant geometrically non-linear theory of elastic shells, Int. J. Solids Struct, 51(11), 2133-2143, (2014).

[8] V.A., Eremeyev, L. P.,Lebedev, Existence theorems in the linear theory of micropolar shells. Z. Angew. Math. Mech, **91(6)**, 468-476, (2011).

[9] V.A. Eremeyev, L.P. Lebedev, M.J. Cloud, The Rayleigh and Courant variational principles in the six-parameter shell theory, Mathematics and Mechanics of Solids, DOI: 10.1177/1081286514553369.

[10] M. Bîrsan and P. Neff, Existence of minimizers in the geometrically non-linear 6-parameter resultant shell theory with drilling rotations, Mathematics and Mechanics of Solids, DOI: 10.1177/1081286512466659.

[11] M. Bîrsan and P. Neff, Existence theorems in the geometrically non-linear 6-parameter theory of elastic plates, J Elast **112**, 185–198 (2013).

[12] J. Chróścielewski, J. Makowski and W. Pietraszkiewicz, Statics and Dynamics of Multifold Shells: Nonlinear Theory and Finite Element Method, in Polish (Wydawnictwo IPPT PAN, Warsaw 2004) .

[13] J. Chróścielewski, J. Makowski and H. Stumpf, Genuinely resultant shell finite elements accounting for geometric and material non-linearity, Int. J. Numer. Meth. Eng. **35**, 63–94, (1992).

[14] J. Chróścielewski, W. Pietraszkiewicz and W. Witkowski, On shear correction factors in the non-linear theory of elastic shells, Int. J. Solids Struct. **47**, 3537–3545 (2010).

[15] J. Chróścielewski and W. Witkowski, 4-node semi-EAS element in 6–field nonlinear theory of shells, Int. J. Numer. Meth. Eng. **68**, 1137–1179 (2006).

[16] J. Chróścielewski, I. Lubowiecka, Cz. Szymczak and W. Witkowski, On some aspects of torsional buckling of thin-walled I-beam columns, Computers and Structures **84**, 1946–1957 **(**2006).

[17] W. Witkowski, 4-Node combined shell element with semi-EAS-ANS strain interpolations in 6-parameter shell theories with drilling degrees of freedom, Computational Mechanics **43**, 307–319, (2009).

MOST WIEDZY Downloaded from mostwiedzy.pl

[18] J. Chróścielewski, I. Kreja, A. Sabik and W. Witkowski, Modeling of composite shells in 6-parameter nonlinear theory with drilling degree of freedom, Mech. Adv. Mater. Struct. **18**, 403–419 (2011).

[19] J.N. Reddy, Mechanics of Laminated Composite Plates and Shells: Theory and Analysis, Second Edition (CRC, Boca Raton, London, New York, Washington D.C. 2003).

[20] S. Burzyński, J. Chróścielewski and W. Witkowski, Elastoplastic material law in 6-parameter nonlinear shell theory, Shell Structures: Theory and Applications, Vol 3, edited by W. Pietraszkiewicz and J. Górski, 377–380 (CRC Press, London 2014).

[21] S. Burzyński, J. Chróścielewski and W. Witkowski, Elastoplastic law of Cosserat type in shell theory with drilling rotation, Mathematics and Mechanics of Solids, DOI: 10.1177/1081286514554351

[22] W. Nowacki, Couple-stresses in the theory of thermoelasticity. In: Irreversible aspects of continuum mechanics and transfer of physical characteristics in moving fluids. IUTAM Symposia Vienna 1966, edited by H. Parkus and L.I. Sedov. 259–278, (Springer-Verlag, Wien, 1968), pdf available at http://bcpw.bg.pw.edu.pl/Content/970/IUTAM_Symposia_Vienna_1966_str259_278.pdf

[23] W. Pietraszkiewicz, J. Badur, Finite rotations in the description of continuum deformation. Int. J. Engineering Sci. **21**, 1097–1115 (1983).

[24] W. Pietraszkiewicz, V.A., Eremeyev, On vectorially parameterized natural strain measures of the non-linear Cosserat continuum. International Journal of Solids and Structures, **46(11)**, 2477-2480, (2009).

[25] Chróścielewski J, Lubowiecka I, Pietraszkiewicz W. FEM and time stepping procedures in non-linear dynamics of flexible branched shell structures. In Theories of Plates and Shells, Kienzler R, Altenbach H, Ott I (eds). Critical Review and New Applications in Lecture Notes in Applied and Computational Mechanics, vol. 16. Springer: Tokyo, Berlin, 2004; 21–28.

[26] J. Chróścielewski and W. Witkowski, Discrepancies of energy values in dynamics of three intersecting plates, Int. J. Numer. Meth. Biomed. Engng. 2010; 26:1188–1202.

[27] R. de Borst, Simulation of strain localization: a reappraisal of the Cosserat continuum, Engineering computations, **8**, 317–322 (1991).

[28] J. Jeong, H. Ramezani, I. Münch, P. Neff, A numerical study for linear isotropic Cosserat elasticity with conformally invariant curvature, Z. Angew. Math. Mech. **89**, No. 7, 552 – 569 (2009).

[29] P. Neff. A geometrically exact Cosserat shell-model including size effects, avoiding degeneracy in the thin shell limit. I. Formal dimensional reduction for elastic plates and existence of minimizers for positive Cosserat couple modulus. Contin. Mech. Thermodyn. 16 (2004), no. 6, 577–628.

MOST WIEDZY Downloaded from mostwiedzy.pl

[30] P. Neff. A geometrically exact planar Cosserat shell-model with microstructure: existence of minimizers for zero Cosserat couple modulus. Math. Models Methods Appl. Sci. 17 (2007), no. 3, 363–392.

[31] P. Neff, K. Chełmiński. A geometrically exact Cosserat shell model for defective elastic crystals. Justification via Γ-convergence. Interfaces Free Bound. 9 (2007), no. 4, 455–492.

[32] P. Neff, Kwon-Il Hong, J. Jeong. The Reissner-Mindlin plate is the Γ -limit of Cosserat elasticity. Math. Models Methods Appl. Sci. 20 (2010), no. 9, 1553–1590.

[33] P. Neff. The Cosserat couple modulus for continuous solids is zero viz the linearized Cauchy-stress tensor is symmetric. Z. Angew. Math. Mech. 86 (2006), no. 11, 892–912.

[34] P. Neff, A. Fischle, I. Münch. Symmetric Cauchy stresses do not imply symmetric Biot strains in weak formulations of isotropic hyperelasticity with rotational degrees of freedom. Acta Mechanica 197 (2008), no. 1-2, 19–30.

[35] O. Sander, P. Neff., M. Bîrsan. Numerical treatment of a geometrically nonlinear planar Cosserat shell model, arXiv:1412.3668v1 [math.NA] 11 Dec 2014.

[36] MacNeal RH, Harder RL, A proposed standard set of problems to test finite element accuracy, Finite Elements in Analysis and Design (1985), 1:3-20.

[37] Y. Başar, Y. Ding, Finite rotation elements for the non-linear analysis of thin shell structures, International Journal of Solids and Structures, vol. 26, pp. 83-97, 1990.

[38] HSL, a collection of Fortran codes for large-scale scientific computation, http://www.hsl.rl.ac.uk/

[39] K. Wiśniewski, Finite rotation shells: Basic equations and finite elements for Reissner kinematics. (Springer, Berlin, 2010).

MOST WIEDZY Downloaded from mostwiedzy.pl

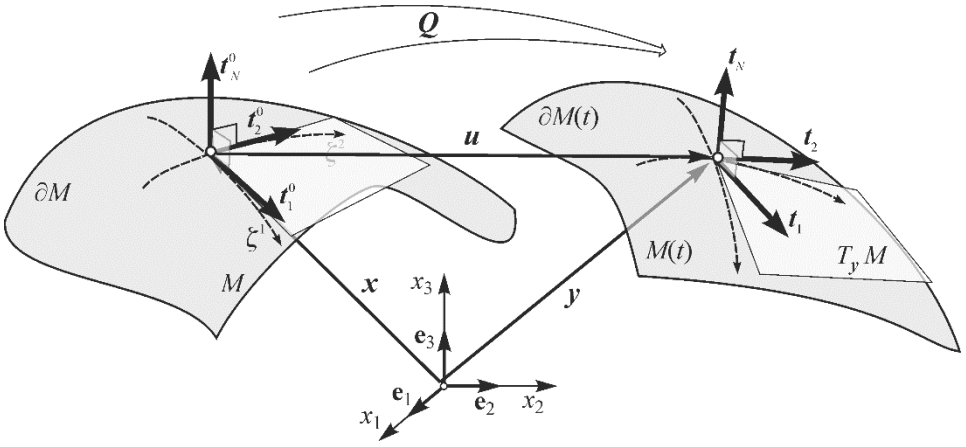

Fig. 1. Kinematics of the shell

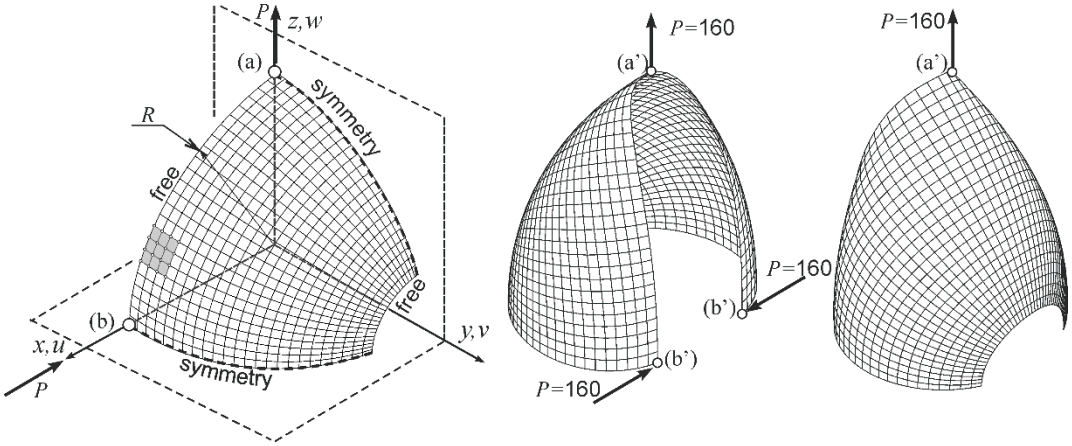

Fig. 2. Pinched hemisphere, geometry and deformed configuration: $\lambda = 16$, $N = \frac{\sqrt{2}}{2}$, $\frac{l}{h_0} = \frac{1}{1000}$,

boundary conditions used as in MacNeal and Harder [36]

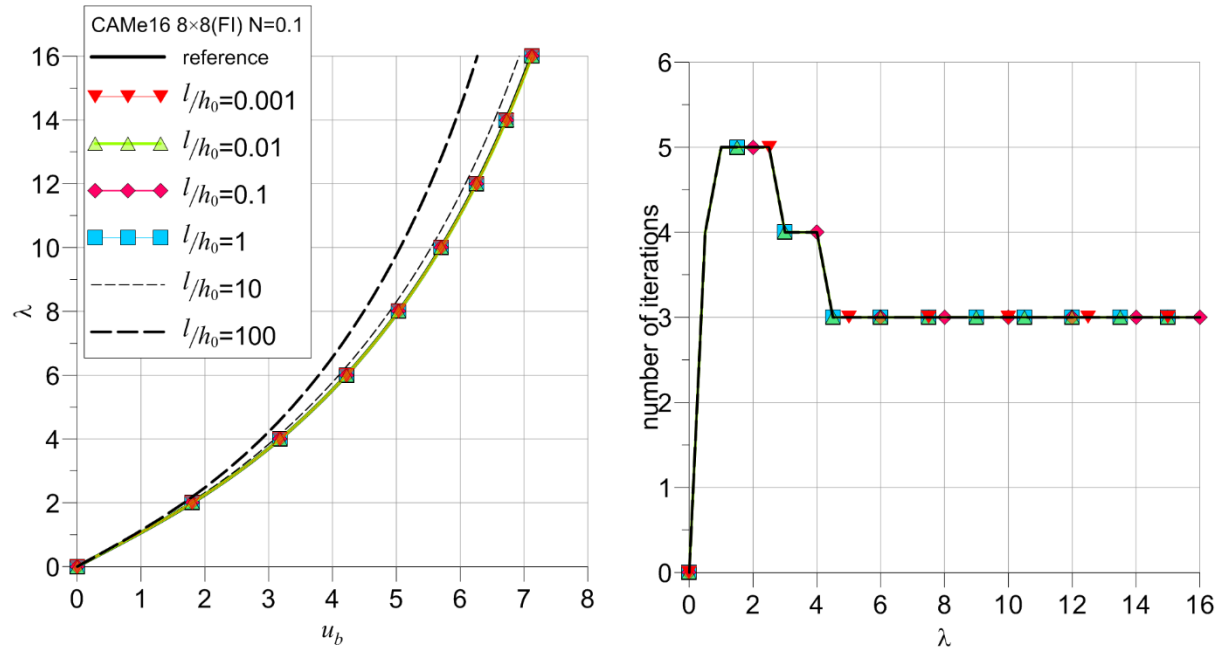

Fig. 3. Pinched hemisphere, $N = 0.1$, variable l: left equilibrium paths, right number of iterations

MOST WIEDZY Downloaded from mostwiedzy.pl

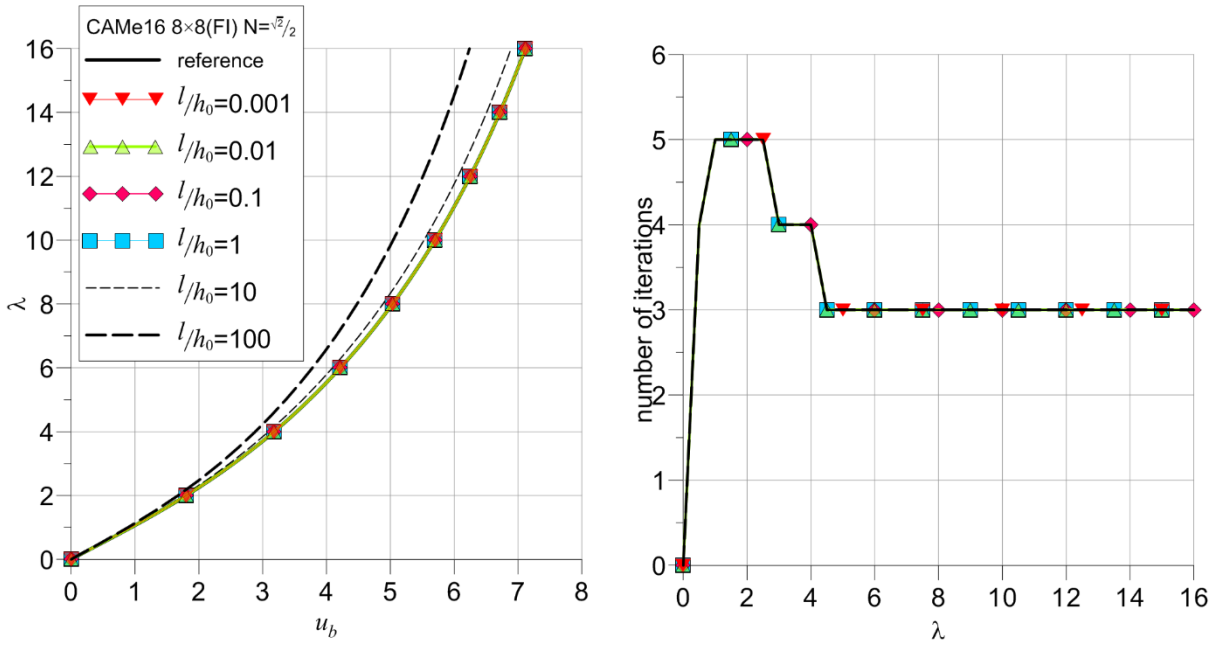

Fig. 4. Pinched hemisphere, $N = \sqrt{2}/2$, variable l, left equilibrium paths, right number of iterations

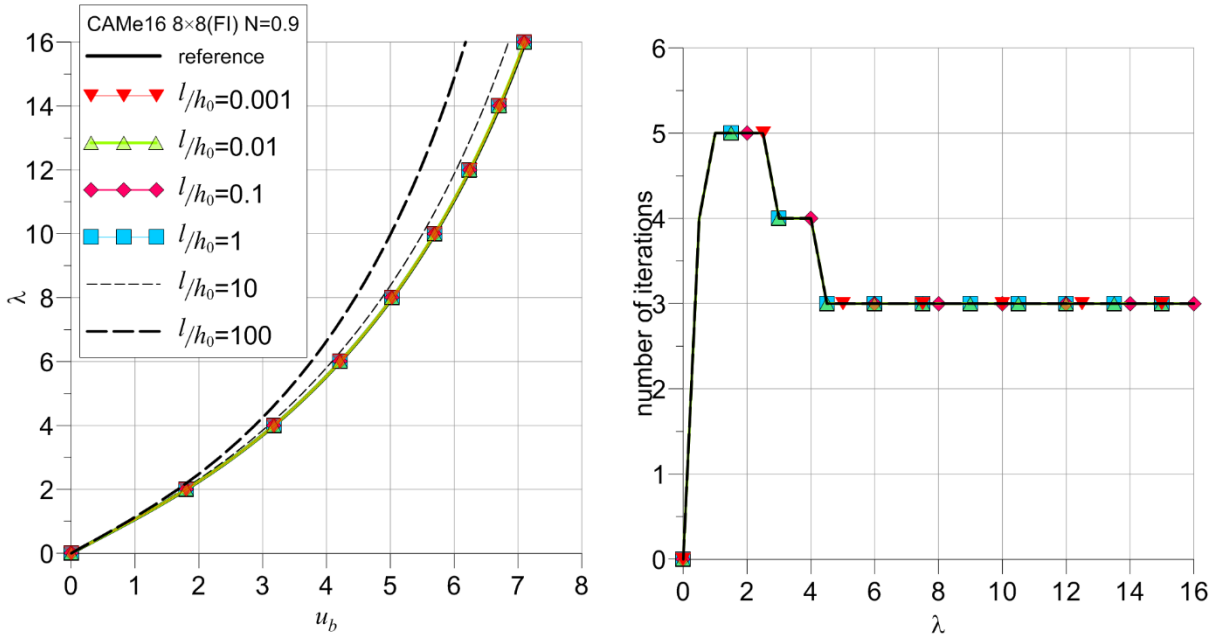

Fig. 5. Pinched hemisphere, $N = 0.9$, variable l, left equilibrium paths, right number of iterations

MOST WIEDZY Downloaded from mostwiedzy.pl

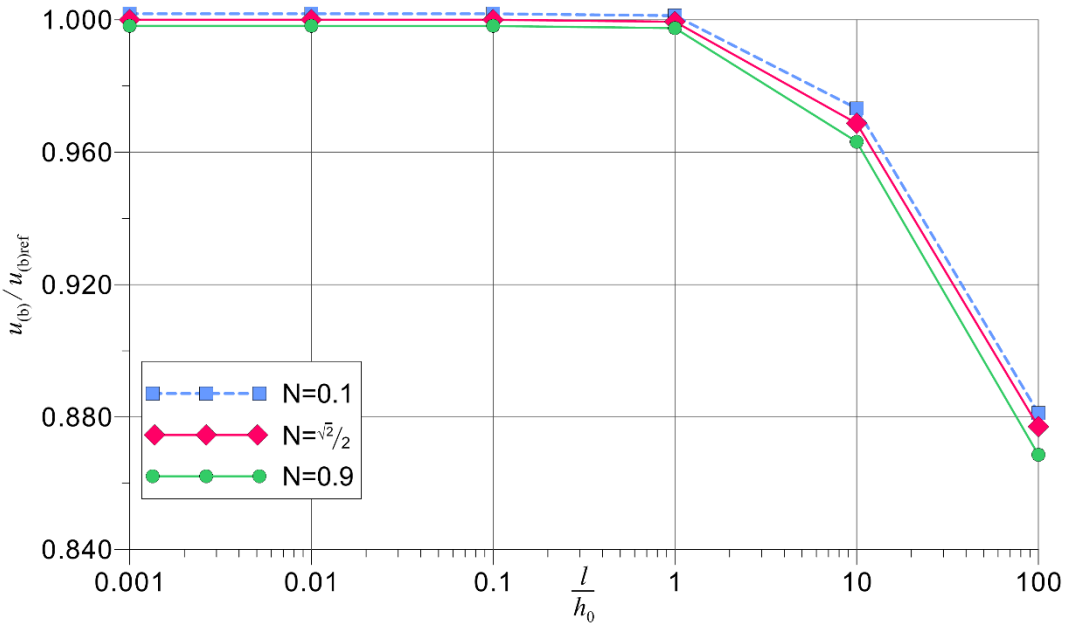

Fig. 6. Pinched hemisphere, variable N, variable l, normalized displacement u_b, $\lambda = 16$

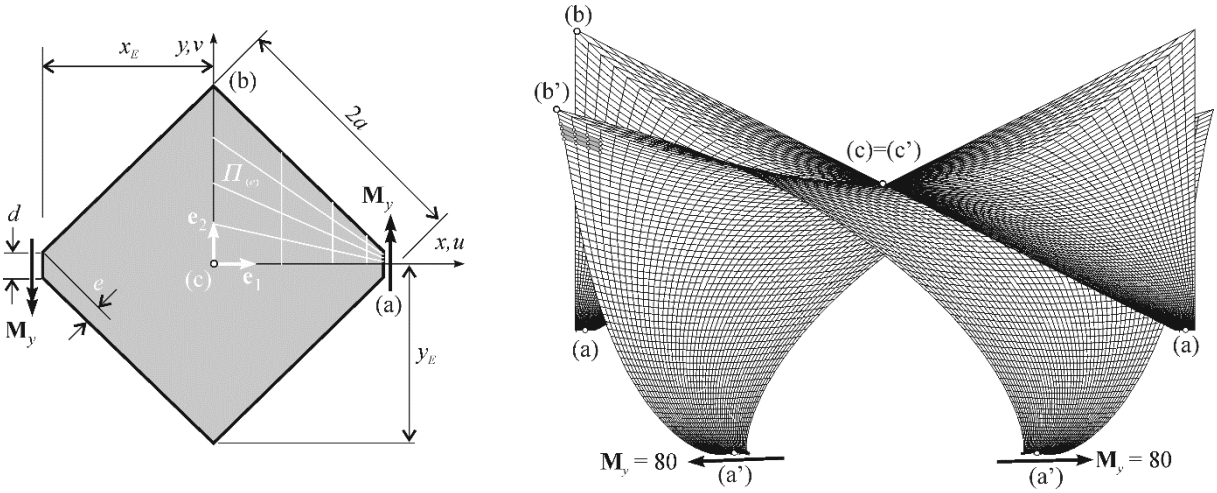

Fig. 7. Hyperbolic paraboloidal shell, geometry and deformed configuration: $\lambda = 16$, $N = \frac{\sqrt{2}}{2}$,

$\frac{l}{h_0} = \frac{1}{1000}$

MOST WIEDZY Downloaded from mostwiedzy.pl

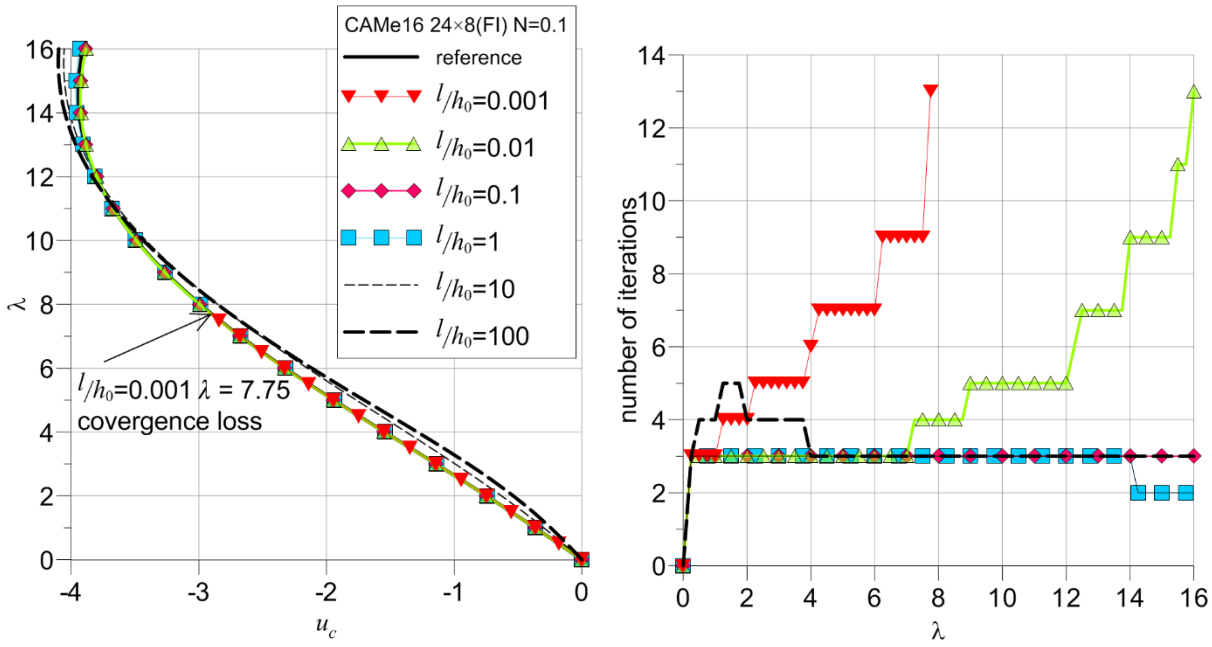

Fig. 8. Hyperbolic paraboloidal shell, $N = 0.1$, variable l, left equilibrium paths, right number of iterations

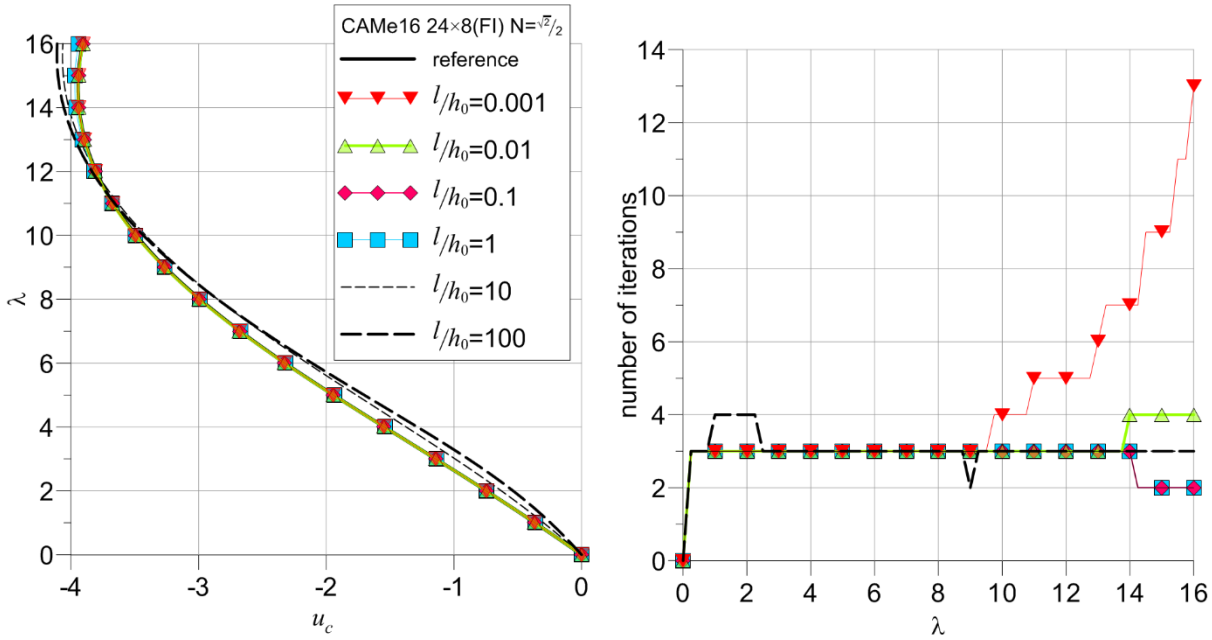

Fig. 9. Hyperbolic paraboloidal shell, $N = \frac{\sqrt{2}}{2}$, variable l, left equilibrium paths, right number of iterations

MOST WIEDZY Downloaded from mostwiedzy.pl

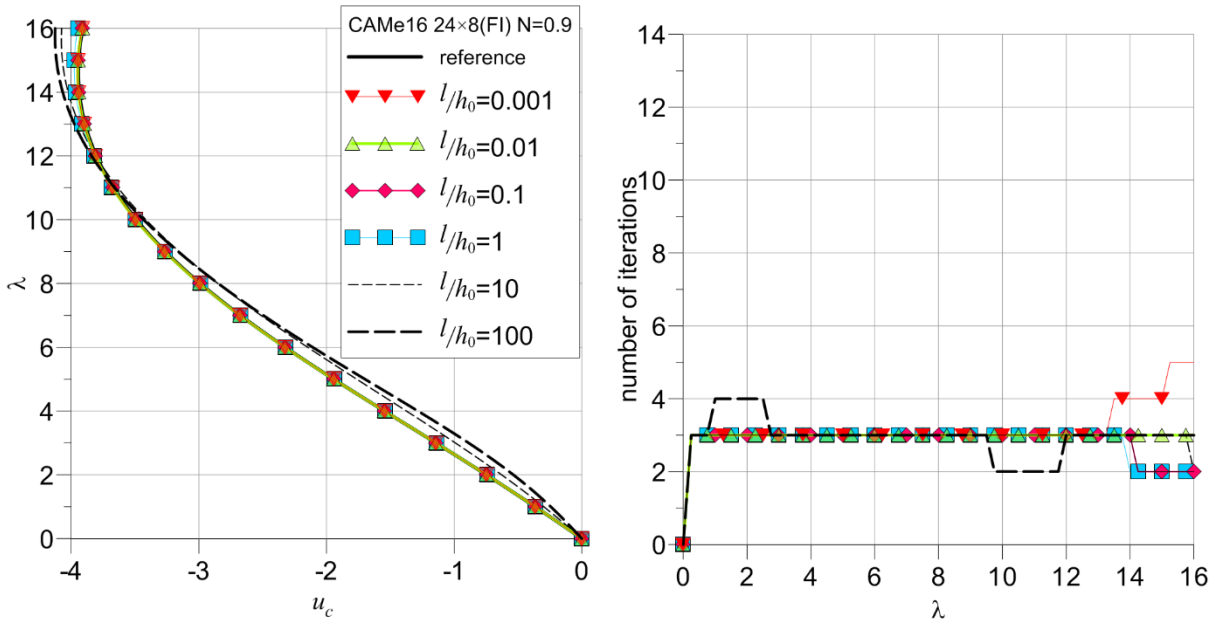

Fig. 10. Hyperbolic paraboloidal shell, $N = 0.9$, variable l, left equilibrium paths, right number of iterations

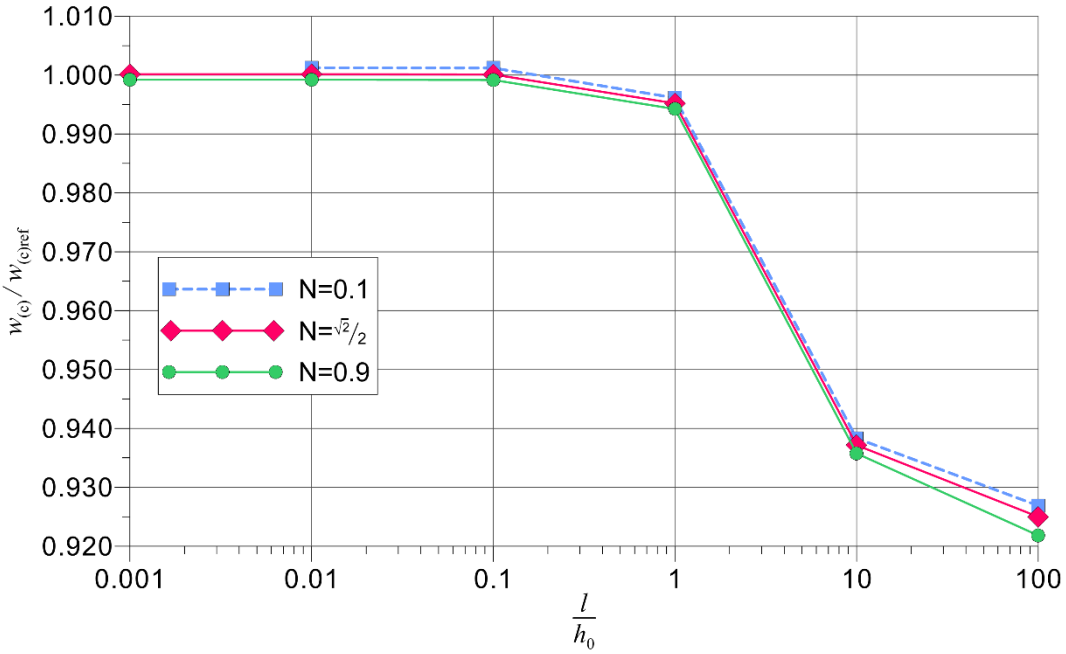

Fig. 11. Hyperbolic paraboloidal shell, variable N, variable l, normalized displacement w_c, $\lambda = 16$

MOST WIEDZY Downloaded from mostwiedzy.pl

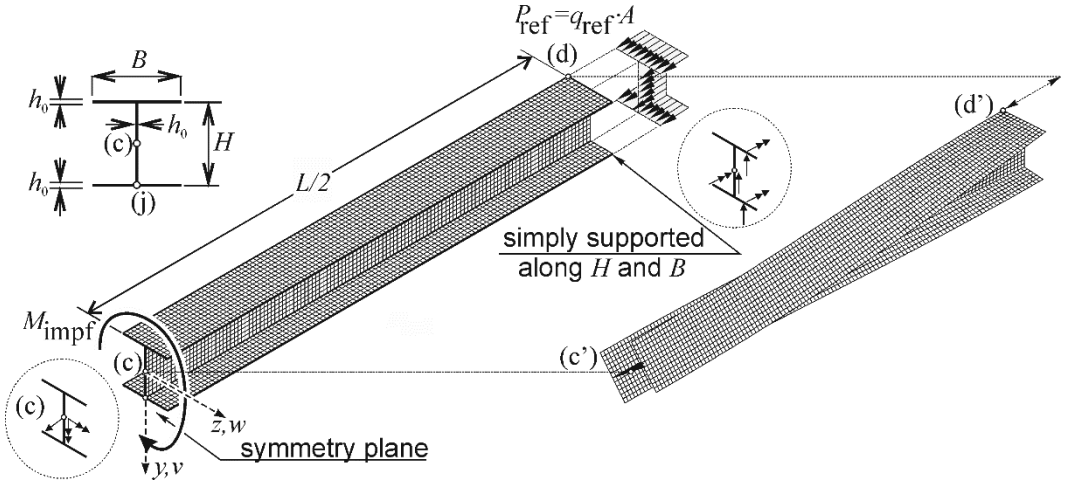

Fig. 12. I-beam column, geometry and deformed configuration: $\lambda = 3.91513$, $N = \frac{\sqrt{2}}{2}$, $\frac{l}{h_0} = \frac{1}{1000}$,

arrows shown in circled cross-sections denote imposed boundary conditions (BC), BC at point c) applies to all nodes at beam axis, BC at point d) applies to the nodes placed on the upper, lower flange and on the web

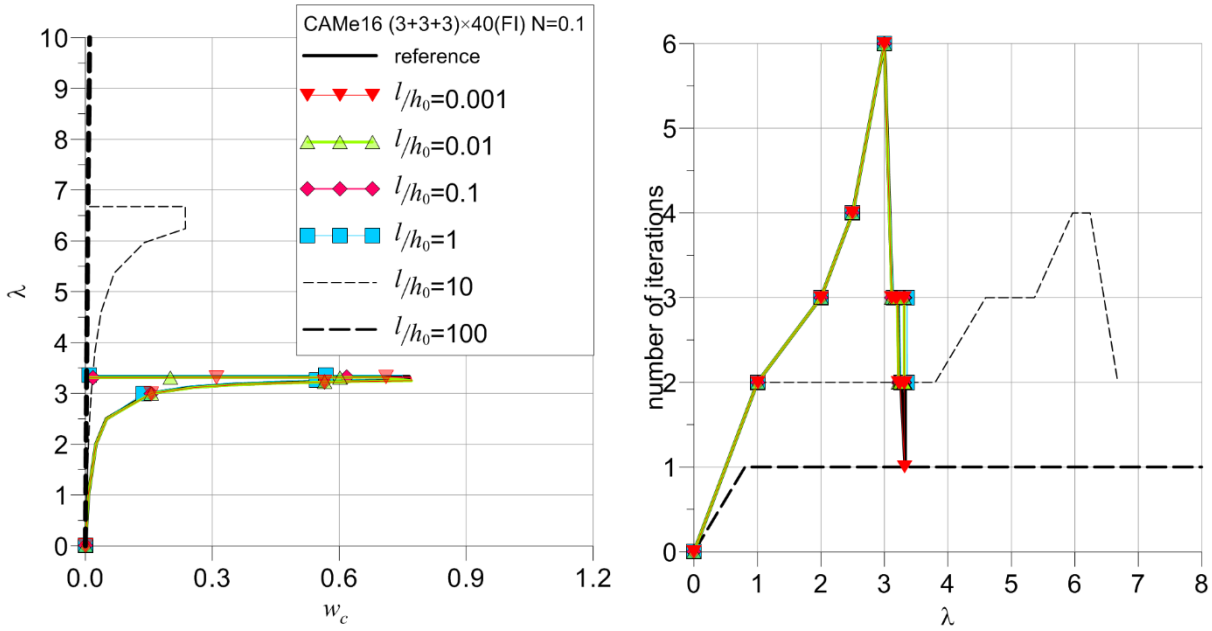

Fig. 13. I-beam column, $N = 0.1$, variable l, left equilibrium paths, right number of iterations

MOST WIEDZY Downloaded from mostwiedzy.pl

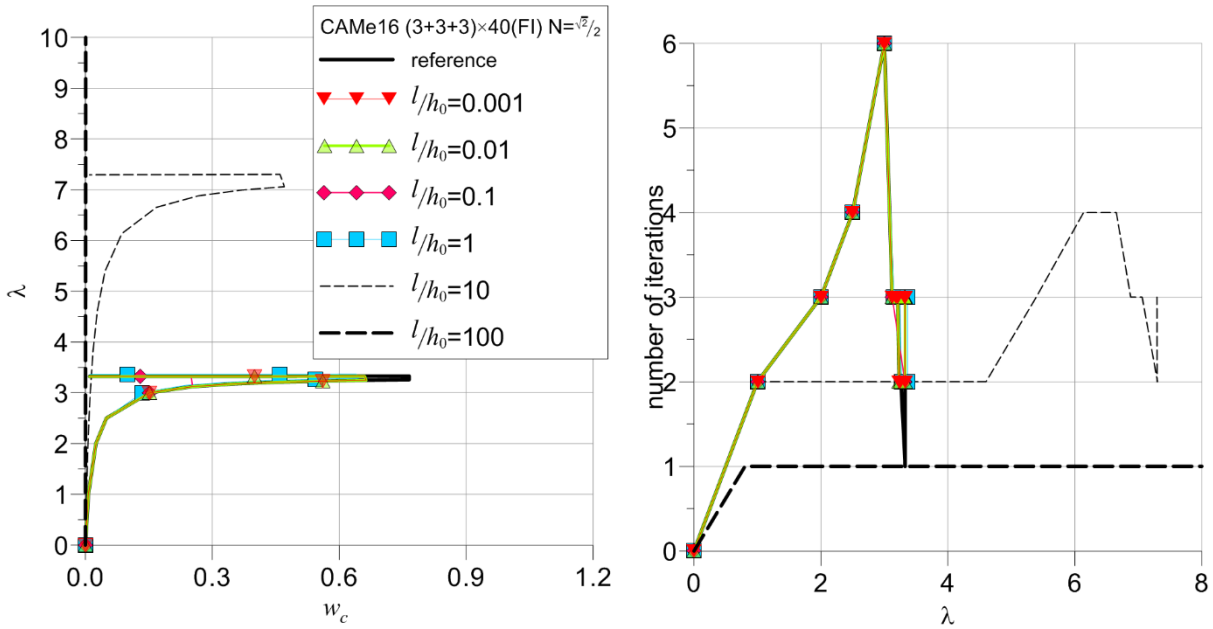

Fig. 14. I-beam column, $N = \frac{\sqrt{2}}{2}$, variable l, left equilibrium paths, right number of iterations

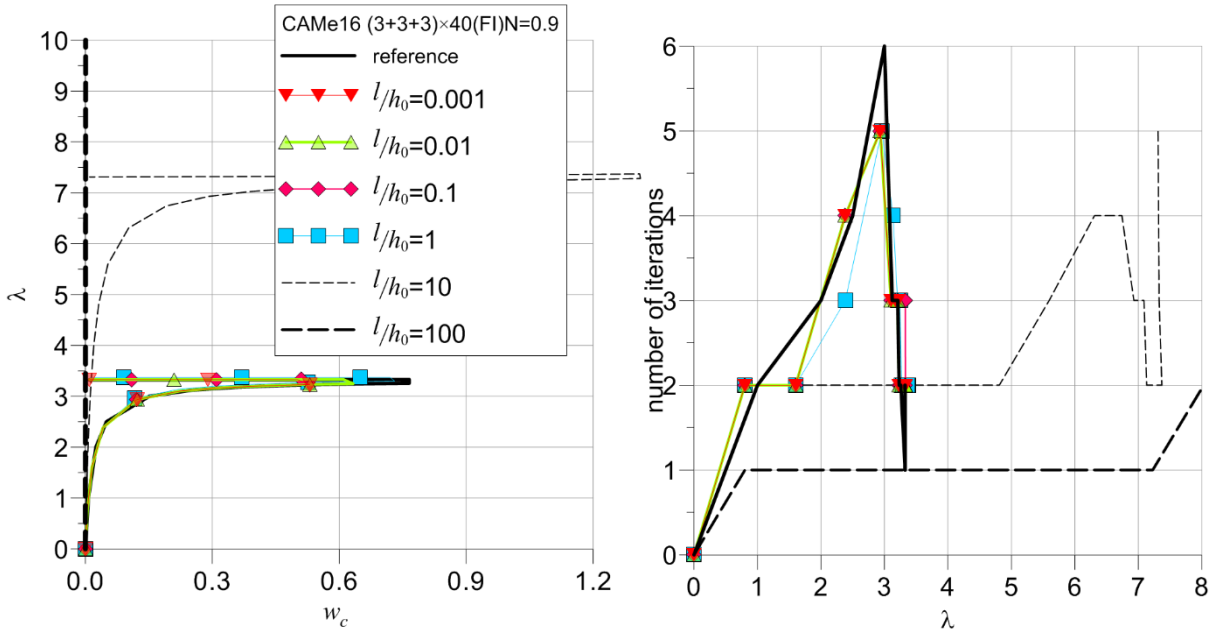

Fig. 15. I-beam column, $N = 0.9$, variable l, left equilibrium paths, right number of iterations

MOST WIEDZY Downloaded from mostwiedzy.pl

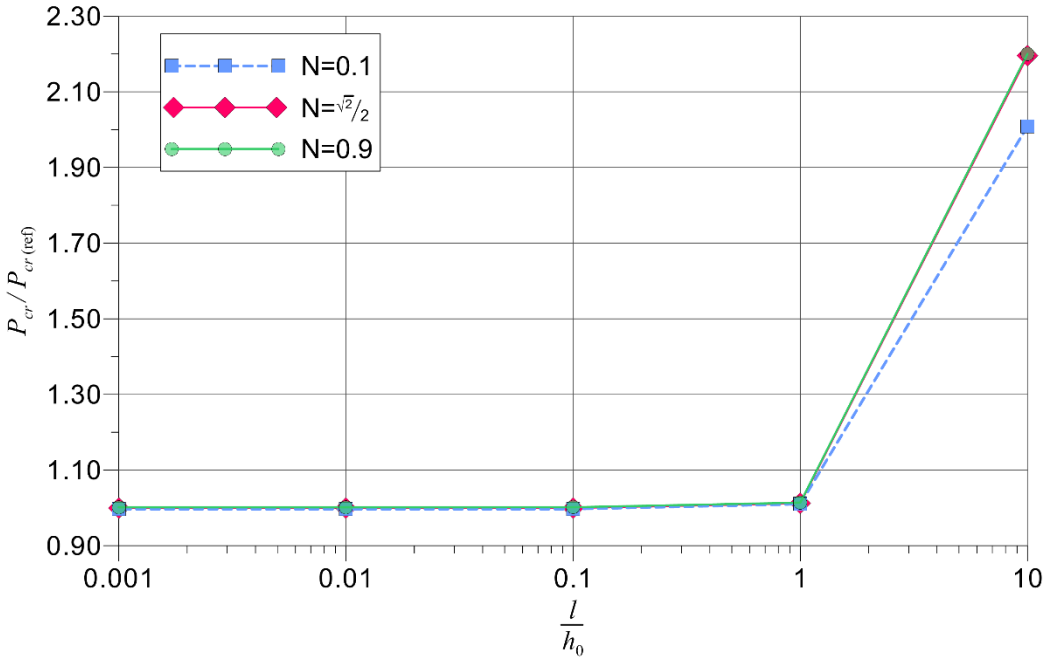

Fig. 16. I-beam column, variable N, variable l, normalized torsional buckling load

MOST WIEDZY Downloaded from mostwiedzy.pl